Carbon Nanotube Sidewall Functionalization with Carbonyl Compounds—Modified Birch Conditions vs the Organometallic Reduction Approach

Benjamin Gebhardt,[†] Zois Syrgiannis,[†] Claudia Backes,[†] Ralf Graupner,[‡] Frank Hauke,[†] and Andreas Hirsch*,[†]

[†]Department of Chemistry and Pharmacy and Institute of Advanced Materials and Processes (ZMP), University of Erlangen-Nuremberg, Henkestrasse 42, 91054 Erlangen, Germany

[‡]Technische Physik, Universität Erlangen-Nürnberg, Erwin-Rommel-Strasse 1, 91058 Erlangen, Germany

S *Supporting Information*

ABSTRACT: Covalent addition reactions turned out to be one of the most important functionalization techniques for a structural alteration of single walled carbon nanotube (SWCNT) scaffolds. During the last years, several reaction sequences based on an electrophilic interception of intermediately generated $SWCNT^{n-}$ carbanions, obtained via Birch reduction or by a nucleophilic addition of organometallic species, have been developed. Nevertheless, the scope and the variety of potential electrophiles is limited due to the harsh reaction conditions requested for a covalent attachment of the functional entities onto the SWCNT framework. Herein, we present a significant modification of the reductive alkylation/arylation sequence, the so-called Billups reaction, which extends the portfolio of electrophiles for covalent sidewall functionalization to carbonyl compounds—ketones, esters, and even carboxylic acid chlorides. Moreover, these carbonyl-based electrophiles can also be used as secondary functionalization reagents for anionic SWCNT intermediates, derived from a primary nucleophilic addition step. This directly leads to the generation of mixed functional SWCNT architectures, equipped with hydroxyl or carbonyl anchor groups, suitable for ongoing derivatization reactions. A correlated absorption and emission spectroscopic study elucidates the influence of the covalent sidewall functionalization degree onto the excitonic transition features of carbon nanotubes. The characterization of the different SWCNT adducts has been carried out by means of Raman, UV−vis/nIR, and fluorescence spectroscopy as well as by thermogravimetric analysis combined with mass spectrometry and X-ray photoelectron spectroscopy analysis.
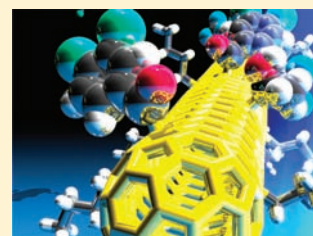
INTRODUCTION

Until the 1980's of the last century, the carbon universe was built on the well-known modifications graphite and diamond. This perspective totally changed with the discovery of the molecular carbon allotropes fullerenes,[1] carbon nanotubes (CNTs),[2−4] and graphene.[5] Based on the outstanding thermal, mechanical, and electronic properties of carbon nanotubes, still unprecedented for any other nanostructured material,[6,7] interest in the investigation and the modification of this novel carbon allotrope arose immediately. Realizing this remarkable potential, a variety of possible applications as future electronic devices or as single molecule sensors and fuel storage materials have been envisaged.[8] Nevertheless, in order to pave the road for CNT applications several hurdles had to be overcome related to the intrinsic poor solubility of single walled carbon nanotubes (SWCNTs) in organic and aqueous solvents.[9,10] It was rapidly recognized that chemical functionalization is a keystone in resolving this task. The chemical modification of the carbon framework of CNTs can: (a) improve their solubility, (b) modify and fine-tune the physical properties of carbon nanotubes and their derivatives, (c) combine the extraordinary properties of CNTs with the properties of other compound classes, and as a consequence, (d) can open the door for the entry of carbon nanotubes into CNT-based technological applications.

Therefore, the chemists' tool box has been equipped with a couple of sidewall functionalization sequences which have been nicely illustrated in a series of review articles related to that topic.[11−16] One widely used method for the introduction of sidewall addends is the nucleophilic addition of organolithium[17−19] and organomagnesium compounds.[20] The primary addition step generates charged anionic nanotube species, which can be used for a secondary functionalization by the reaction with styrene,[21] chlorinated polypropylene, and N-formylpiperidine[23] or a variety of alkyl halogenides,[24,25] yielding mixed functional SWCNT derivatives (Scheme 1a). These types of doubly functionalized SWCNT architectures are also accessible by a reductive retro-functionalization sequence, recently described by our group.[26]

Another commonly used sidewall functionalization reaction, which is also based on negatively charged SWCNT intermediates, is the reductive alkylation[27,28] and arylation[29] under Birch

Scheme 1. SWCNT Architectures[a]
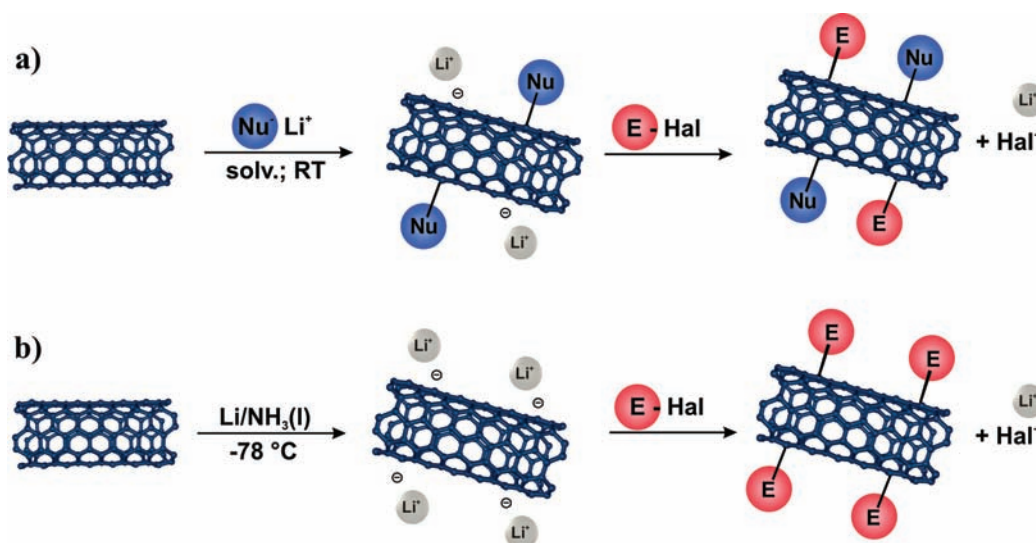
[a] (a) Electrophilic trapping of negatively charged $(Nu)_n$$-$$SWCNT^{n-}$ intermediates obtained by the primary addition of a nucleophile. (b) Reductive SWCNT functionalization by electrophiles via Birch-reduced $SWCNT^{n-}$ species.

conditions, introduced by Billups and co-workers (Scheme 1b). Herein, CNTs are reduced in liquid ammonia by lithium metal and reacted with different alkyl or aryl halogenides[30−32] as electrophilic addend species. Based on a single electron transfer (SET) reaction with the charged SWCNTs as donor components, the corresponding carbon centered alkyl/aryl radicals are generated, which subsequently attack the sp^2 network of the carbon nanotubes. Furthermore, this reaction sequence has been adapted in order to attach nitrogen, oxygen, and sulfur centered radicals to SWCNTs.[33,34] In spite of the various results reported for this reductive functionalization sequence, the harsh reaction conditions with free electrons in liquid ammonia limit the scope of the functional diversity of the applied electrophilic species. It has been outlined by Borondics et al. that under these highly reactive conditions, competing side reactions, like the protonation of the charged SWCNTs, take place.[35,36] Therefore, efforts have been taken to substitute the highly aggressive reaction medium by inert solvents. These methods rely on electron-transfer reagents, like lithium naphthalenide[35−39] or di-*tert*-butyl-biphenyl,[40] to generate the negatively charged SWCNT intermediates. However, the applied electron-transfer mediators tend to adsorb to the nanotube sidewalls by $\pi$$-$$\pi$-interactions, due to their aromatic character, and cannot easily be removed after SWCNT functionalization.

In the present study, we extended the portfolio of electrophiles for the reductive SWCNT functionalization to ketones, esters, and carboxylic acid chlorides, by a significant modification of the Birch conditions, yielding highly functionalized SWCNT derivatives, equipped with hydroxyl or keto functionalities as a platform for subsequent functionalization reactions. Our reaction sequence is based on the inert solvent THF, whereas the charged SWCNT intermediates are generated easily and efficiently in liquid ammonia. The introduced compound classes can also be used for the electrophilic interception of the negatively charged SWCNT intermediates generated by the nucleophilic attack of organolithium species yielding mixed functional SWCNT architectures. In addition, we were able to show that

the functionalization degrees for the SWCNT derivatives produced by the reductive functionalization sequence under modified Birch conditions exhibit a direct correlation with the stability/reactivity of the intermediately generated ketyl radical species. Moreover, an absorption and emission spectroscopic study, based on the dispersible SWCNT derivatives with varying sidewall functionalization degree, elucidates the influence of the covalent framework alteration onto the excitonic transition features of carbon nanotubes. Characterization of the functional SWCNT adducts has been carried out by means of Raman, UV−vis/nIR, and fluorescence spectroscopy as well as by thermogravimetric analysis/mass spectrometry (TGA/MS) and X-ray photoelectron spectroscopy (XPS) analysis analysis.

■ EXPERIMENTAL SECTION

Materials. SWCNTs produced by the HiPco process were obtained from Unidym (lot number P0355; grade: pure; TGA residue 5 wt %) and used as received without any further treatment. Chemicals and solvents were purchased from Acros (Geel, Belgium), Sigma Aldrich Co. (Munich, Germany), and Merck KGaA (Darmstadt, Germany) and used as received.

Trapping of $SWCNT^{n-}$ Intermediates with Carbonyl-Based Electrophiles. In a heat-dried and argon-purged four-necked round-bottomed flask (250 mL) equipped with two gas inlets and pressure compensation HiPco SWCNTs (5 mg, 0.42 mmol of carbon) were dispersed in 100 mL anhydrous THF by 30 min ultrasonication. The flask with the dispersion was cooled to −78 °C (acetone/dry ice), and ammonia (100 mL) was condensed. Afterward, lithium metal (14.56 mg, 2.08 mmol, 5 equiv in relation to mole carbon SWCNT) was added to the SWCNT dispersion, and the reaction mixture was stirred for 1 h yielding a stable blue-black dispersion. The cooling was removed, and the solution was kept stirring until the complete evaporation of the ammonia. The resulting lithium bronze was removed by a syringe, and the dispersion was ultrasonicated for additional 30 min. Subsequently, 2 equiv [referred to lithium (4.16 mmol)] of the carbonyl-based electrophile [acetophenone (**1**), 1,1,1-trifluoroacetone (**2**), methyl benzoate (**3**), methyl trifluoroacetate (**4**), 3,4-dichlorobenzoyl chloride (**5**)] were added to the dispersion, and the reaction mixture was stirred overnight. In a separation funnel, water (100 mL) and cyclohexane

7986

dx.doi.org/10.1021/ja2016872 |*J. Am. Chem. Soc.* 2011, 133, 7985–7995

(100 mL) were added to the THF dispersion. The water/THF phase was discarded, and the cyclohexane layer with the functionalized nanotubes was purged two times with water and THF (100 mL), respectively. The organic layer with the functionalized nanotubes was filtered through a reinforced cellulose membrane filter with a pore size of 0.2 μm (Sartorius) and thoroughly washed with THF, iso-propanol, ethanol, and water, 250 mL each. The resulting black solid was dried in a vacuum oven at 75 °C overnight.

Trapping of (^{n}Bu)$_n$-SWCNT^{n-} Intermediates with Carbonyl-Based Electrophiles. In a heat-dried and nitrogen-purged four-necked round-bottomed flask (250 mL) equipped with two gas inlets and pressure compensation HiPco SWCNTs (5 mg, 0.42 mmol of carbon) were dispersed in 100 mL anhydrous THF by 30 min ultrasonication. Afterward, 5 equiv (in relation to mole carbon SWCNT) of n-butyl lithium (0.92 mL, 2.08 mmol) were added drop wisely. The dispersion was stirred at room temperature for 5 h. Subsequently, 2 equiv [referred to n-butyl lithium (4.16 mmol)] of the carbonyl-based electrophile [acetophenone (**1**), 1,1,1-trifluoroacetone (**2**), methyl benzoate (**3**), methyl trifluoroacetate (**4**), 3,4-dichlorobenzoyl chloride (**5**)] were added to the dispersion, and the reaction mixture was stirred overnight. In a separation funnel, water (100 mL) and cyclohexane (100 mL) were added to the THF dispersion. The water/THF phase was discarded, and the cyclohexane layer with the functionalized nanotubes was purged two times with water and THF (100 mL), respectively. The organic layer with the nanotubes was filtered through a reinforced cellulose membrane filter with a pore size of 0.2 μm (Sartorius) and thoroughly washed with THF, iso-propanol, ethanol, and water, 250 mL each. The resulting black solid was dried in a vacuum oven at 75 °C overnight.

Microwave-Based Purification of SWCNTs According to Literature[41]. In a microwave vessel, 20 mg as received HiPco SWCNTs (1.66 mmol of carbon) were suspended in 5 mL CH_2Cl_2 and sealed. In the following, the suspension was heated to 150 °C under microwave irradiation (300 W, 16 bar), and the temperature was kept constant for 4 min. The resulting black dispersion was transferred to a culture dish. The precipitated metal-containing particles were removed, and the remaining SWCNT dispersion was filtrated over a 0.2 μm pore size regenerated cellulose filter (Sartorius) and washed with CH_2Cl_2. The entire procedure was repeated three times to increase the purity of the SWCNT sample.

Thermal Purification of SWCNTs according to Literature[42]. In a ceramic crucible, 100 mg as received HiPco SWCNTs (8.33 mmol of carbon) were weighted out, and the crucible was placed in a quartz Schlenk tube equipped with a quartz cab with two gas inlets. Afterward, a gas flow of wet air (compressed air passed through a water bubbler) was passed over the sample with a constant flow rate of 100 mL/min. The SWCNT sample was heated three times at temperatures of 225 °C (18 h), 325 °C (1.5 h), and 425 °C (1 h) in a tube furnace. Between the heating steps, the sample was dispersed in concentrated HCl (15 min ultrasonication) and stirred overnight. The color of the HCl hereby turned from colorless to yellow, indicating the dissolution of iron impurities. The SWCNTs were filtered over a 0.2 μm pore size cellulose nitrate filter (Whatman), dried in a vacuum oven at 75 °C for 3 h, and transferred to the ceramic crucible for the next heating step. After the third heating and washing cycle, the SWCNTs were placed in the furnace again and annealed at 800 °C under Ar atmosphere (1 h).

Trapping of SWCNT^{n-} Intermediates with Carbonyl-Based Electrophiles after Purification. In a heat-dried and nitrogen-purged four-necked round-bottomed flask (250 mL) equipped with two gas inlets and pressure compensation microwave purified HiPco SWCNTs (*MW*-SWCNTs) or thermally purified HiPco, SWCNTs (*TH*-SWCNTs) (15 mg, 1.25 mmol of carbon) were dispersed in 150 mL anhydrous THF by 30 min ultrasonication. The flask with the dispersion was cooled to −78 °C (acetone/dry ice), and ammonia (100 mL) was condensed. Afterward, lithium metal (43.38 mg, 6.25 mmol, 5 equiv in relation to mole carbon SWCNT) was added to the SWCNT dispersion, and the

reaction mixture was stirred for 1 h yielding a stable blue-black dispersion. The cooling was removed, and the solution was kept stirring until the complete evaporation of the ammonia. The resulting lithium bronze was removed by a syringe, and the dispersion was ultrasonicated for additional 30 min. Subsequently, 2 equiv [referred to lithium (12.5 mmol)] of the carbonyl-based electrophile [acetophenone (**1**) and methyl benzoate (**3**)] were added to the dispersion, and the reaction mixture was stirred overnight. In a separation funnel, water (100 mL) and cyclohexane (100 mL) were added to the THF dispersion. The water/THF phase was discarded, and the cyclohexane layer with the functionalized nanotubes was purged two times with water and THF (100 mL), respectively. The organic layer with the functionalized nanotubes was filtered through a reinforced cellulose membrane filter with a pore size of 0.2 μm (Sartorius) and thoroughly washed with THF, iso-propanol, ethanol, and water, 250 mL each. The resulting black solid was dried in a vacuum oven at 75 °C overnight.

Instruments and Measurements. Raman spectroscopic characterization was carried out on a Horiba Jobin Yvon LabRAM Aramis confocal Raman microscope (excitation wavelengths: 532, 633, and 785 nm) with a laser spot size of ~1 μm (Olympus LMPlanFl 100x, NA 0.80). The incident laser power was kept as low as possible to avoid structural sample damage: 240 μW (532 nm), 114 μW (622 nm), and 3 mW (785 nm). Raman mappings were recorded with SWIFT Ultra Fast Raman Imaging (Horiba). The presented and analyzed Raman spectra were averaged from 15 individual spectra taken at different locations of the buckypapers.

TGA equipped with a MS was performed on a Netzsch STA 409 CD instrument equipped with a Skimmer QMS 422 mass spectrometer (MS/EI) with the following programmed time-dependent temperature profile: 24−100 °C with 10 K/min gradient, isothermic stabilization for 1 h, 100−700 °C with 10 K/min gradient, and isothermic stabilization for 1 h and cooling to 24 °C. The initial sample weights were about 5−10 mg, and the whole experiment was executed under inert gas atmosphere with a He gas flow of 80 mL/min (for the determination of the purification grade oxygen was used under equal conditions).

X-ray induced photoelectron spectra (XPS) were measured on a buckypaper of the respective material. As photon source a monochromatized Al K$_\alpha$ small spot X-ray source was used ($\hbar\omega$ = 1486.6 eV). All binding energies refer to the Fermi-level, which was regularly calibrated using the Au 4f 7/2 core level at 84.00 eV. Peak fitting was carried out with Origin 8.0 using a Voigt peak function.

UV−vis (400−900 nm) and nIR (900−1400 nm) absorption spectra were obtained on a Perkin-Elmer Lambda 1050 spectrophotometer. The functionalized SWCNT material was redispersed in N-methyl-2-pyrrolidone (NMP) (0.1 g/L) by ultrasonication for 30 min. Spectra were taken from the supernatant after mild centrifugation (10 krpm, 10 min, Sigma 4K15) in order to remove coarse aggregates. The concentrations of SWCNTs in the supernatant solutions were calculated with the extinction coefficient reported elsewhere.[43]

Fluorescence spectra were recorded with an NS1 Nano-Spectralyzer from Applied NanoFluorescence LLC (λ_{ex} = 660 and 785 nm). The material for the fluorescence spectroscopic measurements was prepared analogously to the UV−vis/nIR samples and diluted to an optical density of 0.34 at 660 nm (concn = 0.01 g/L).

Atomic force microscopy tapping mode images were recorded on a Solver Pro scanning probe microscope (NT-MDT) equipped with a Sony Exwave HAD camera optical zoom (6.5). The SWCNT dispersion in NMP were spin casted on Si/SiO$_2$ wafers, and areas of interest were localized by the optical interference contrast arising from the opaque bilayered substrate (see Supporting Information and ref 44). The optical microscopic images were acquired with a Zeiss Axio Imager M1m equipped with a Zeiss AxioCam MRc5 under white light illumination (100 W halogen lamp, HAL100) using bright field imaging modes and 0.80 NA objectives.
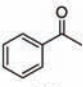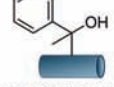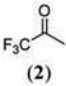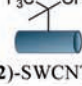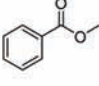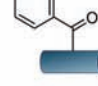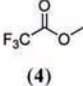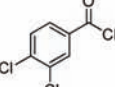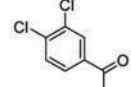
Electrophile (E)	Reductive Functionalization under modified Birch conditions	
(1) acetophenone	f-(1)-SWCNT	A_D/A_G[a]: 1.13 c(NMP): 63 mg/L (63 %) mass loss (coval.)[b]: 2.8% mass loss (compl.)[c]: 2.5% func.degr.(TGA): 0.3%
(2)	f-(2)-SWCNT	A_D/A_G[a]: 2.31 c(NMP): 10 mg/L (10 %) func.degr.(XPS): 0.4%[d]
(3)	f-(3)-SWCNT	A_D/A_G[a]: 1.55 c(NMP): 42 mg/L (42 %) mass loss (coval.)[b]: 6.0% mass loss (compl.)[c]: 7.6% func.degr. (TGA): 0.8%
(4)	f-(4)-SWCNT	A_D/A_G[a]: 2.36 c(NMP): 10 mg/L (10 %)
(5)	f-(5)-SWCNT	A_D/A_G[a]: 1.54 c(NMP): 19 mg/L (19 %) func.degr.(XPS): 0.3%[d]

Figure 1. Tabular representation of the different electrophiles, the corresponding SWCNT derivatives, the Raman determined A_D/A_G values, the concentration of SWCNTs in the supernatant after mild centrifugation with an initial concentration of 0.1 g/L, and the corresponding dispersion efficiency as well as the TGA-based mass loss together with the corresponding functionalization degree. (a) Values are the ratios $A_{D(sample)}/A_{G(sample)}$ related to A_{D0}/A_{G0} of the pristine HiPco SWCNTs. (b) Mass loss detected by TGA in the temperature range between 350 and 570 °C (covalent detachment of substituents); corrected by the mass loss of the pristine HiPco material. (c) Mass loss over the complete temperature range: 100−700 °C; corrected by the mass loss of the pristine HiPco material. (d) Calculation of the degree of functionalization from the XPS spectra was performed according to literature.[45]

X-band electron paramagnetic resonance (EPR) spectroscopy was performed on a JEOL JES-FA 200 apparatus; standard: Mn^{2+}.

Ultrasonications were performed with a Branson 2510-DTH ultrasonic processor (42 kHz, 239 W).

■ RESULTS AND DISCUSSION

A fundamental drawback of the reductive alkyl- and arylation of SWCNTs under classical Birch conditions represents the highly reductive and reactive environment in liquid ammonia. Therefore, molecules sensitive to such harsh reaction conditions, i.e., carbonyl compounds, cannot be used for SWCNT sidewall derivatization. In order to establish an access to a large variety of structurally different electrophiles, we modified the reaction conditions by the substitution of ammonia with THF. SWCNTs were dispersed under ultrasound agitation in dry THF, and the reductive conditions were subsequently established by condensing ammonia and by the addition of lithium metal. Afterward, the ammonia was evaporated, and the remaining lithium-bronze was removed yielding a black solution with charged SWCNT species ($SWCNT^{n-}$) without any free electrons in the inert solvent (for further information see Supporting Information, Figure S1). This solution was repeatedly ultrasonicated to guarantee an efficient individualization of the material. Afterward, carbonyl-based electrophiles—acetophenone (1), 1,1,1-trifluoroacetone (2), methylbenzoate (3), methyltrifluoroacetate (4), and 3,4-dichlorobezoyl chloride (5) (two equivalents referred to the amount of lithium)—were added to the homogeneous black reaction mixture, and the subsequent aqueous workup yielded the corresponding sidewall functionalized materials f-(1−5)-SWCNT as outlined in Figure 1.

In total, the electrophilic addition of ketones yields tertiary alcohols, whereas carboxylic acid derivatives lead to acylated carbon nanotube species. The ketones, esters, and acyl chloride used herein are just a representative cross-section of their compound class, and the method should in principle be applicable to any carbonyl compound.

It has been shown that the one-electron reduction of benzophenone by potassium in toluene yields the corresponding radical anion which readily adds to the carbon nanotube sidewall.[46] Herein, the ketyl radical is generated by a one-electron transfer from the potassium to the dissolved benzophenone. Under our modified Birch conditions, the electron-donor species for the generation of the corresponding ketyl radicals are the reduced SWCNT anions. One-electron reduction by THF dissolved electrons can be excluded in our case, as has been demonstrated by EPR spectroscopic investigations (see Figure S1, Supporting Information). In contrast to a reference sample (THF, lithium naphthalenide), no traces of any EPR signal could be detected in the THF solution after the evaporation of ammonia and the removal of the lithium bronze.

The covalent addition of the different ketyl species onto the nanotube scaffold can unambiguously be proven by Raman spectroscopy. This characterization technique has been established as the primary tool for the structural investigation of sidewall functionalized SWCNTs.[47−51] The covalent attachment of functional entities and therefore the rehybridization of sidewall C atoms significantly influences the intensity ratio of the Raman bands. The most prominent spectral change constitutes in an increase in the intensity of the D-band (∼1300 cm^{-1}), which arises from the generation of sp^3-C atoms as defects in the sp^2 carbon lattice, in relation to those of the radial breathing modes
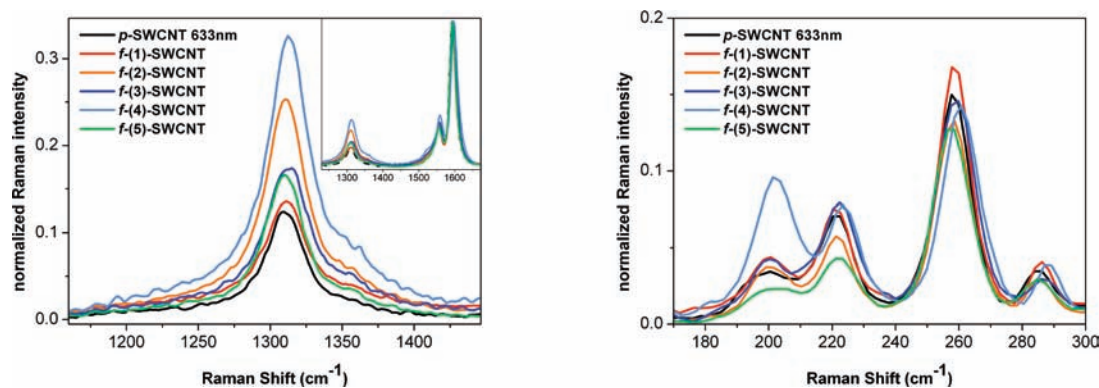
Figure 2. Raman spectra (633 nm excitation) of pristine SWCNTs (black trace) and functionalized SWCNT derivatives f-(**1−5**)-SWCNT (color coded) obtained under modified birch conditions. Left: D-band with D- and G-band regions as inset. Right: RBM region.

(RBMs), $\sim$100−300 cm^{-1}, and the G-band, $\sim$1590 cm^{-1}. The intensity ratio between the D- and the G-bands (A_D/A_G) can therefore be taken as a measure for the extent of functionalization. Multiple Raman spectra were obtained from different spots of the sample, normalized to the G-band and averaged to give a comprehensive picture of the functionalized material. The A_D/A_G ratios were corrected by the A_{D0}/A_{G0} values of the starting SWCNT material. The D-band and the RBM region (excitation wavelength: 633 nm) of the differently functionalized SWCNT derivatives f-(**1−5**)-SWCNT are depicted in Figure 2 (the corresponding spectra for 532 and 785 nm excitation are presented in Figures S2 and Figure S3, Supporting Information, respectively).

In comparison to the pristine starting material, the functionalized SWCNT derivatives f-(**1-5**)-SWCNTs exhibit a pronounced increase of the A_D/A_G ratio (see Figure 2), indicative of a covalent sidewall attachment of the intermediately generated ketyl radicals. Furthermore, a direct correlation between the functionalization degree and the radical stability/reactivity can be derived from the calculated A_D/A_G values. The less stable and higher reactive alkyl substituted ketyl radicals, generated from methyltrifluoroacetate (**4**) and 1,1,1-trifluoroacetone (**2**), yield 2-fold higher A_D/A_G ratios [$A_D/A_G = 2.36$ (**4**) and $A_D/A_G = 2.31$ (**2**)] in comparison with the less reactive phenyl substituted systems, derived from acetophenone (**1**) ($A_D/A_G = 1.13$), methylbenzoate (**3**) ($A_D/A_G = 1.55$), and 3,4-dichlorobezoyl chloride (**5**) ($A_D/A_G = 1.54$), where the spin can be delocalized into the adjacent aromatic moiety for stabilization.

These Raman determined functionalization degrees for the reductive functionalization with carbonyl compounds based on our modified Birch conditions are comparable to the A_D/A_G values for the stoichiometry controlled alkylation and arylation of HiPco SWCNTs recently described by Pénicaud et al.[38] A detailed RBM survey of the Raman spectra in the case of the trapping with methyltrifluoroacetate (**4**) indicates an obvious effect on these spectral features due to a functionalization induced debundling of the sample in combination with size selective addition of the ketyl radical toward small diameter nanotubes. This kind of diameter-dependent functionalization has been observed before for nucleophilic sidewall derivatizations.[19,50] The RBM resonance signals for large diameter SWCNTs (180−250 cm^{-1}) are increased, whereas the resonance intensities for small diameter SWCNTs (250−300 cm^{-1}) are decreased. Raman RBM spectra taken at 532 and 785 nm excitation wavelength support this observation
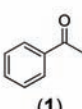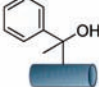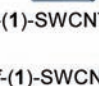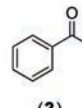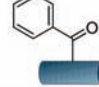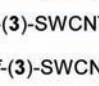

Figure 3. Comparison of the Raman spectroscopic determined functionalization degree (A_D/A_G) of the as received starting material with purified materials after functionalization with two representative electrophiles under modified Birch conditions. (a) Values are the ratios $A_{D(sample)}/A_{G(sample)}$ related to A_{D0}/A_{G0} of the pristine HiPco SWCNTs.

of a size-selective addition reaction. However, we observe no indication on an electronic-type specific discrimination of SWCNTs by ketyl radical addition reactions under these conditions.

In order to evaluate a possible influence of the residual metal impurities (encapsulated in a carbon shell)[52,53] of the as received HiPco material on the reductive functionalization sequence, we purified this material by two independent purification routes, described in literature.[41,42] According to TGA analyses (see Figure S4, Supporting Information) the remaining metal impurities were reduced from 15.0% (p-SWCNTs) to 12.9% (TH-SWCNTs) and 7.0% (MW-SWCNTs), respectively. With these purified material significant increases in the Raman A_D/A_G values of the reductively functionalized derivatives pf-(**1**)-SWCNTs and pf-(**3**)-SWCNTs were obtained. The corresponding functionalization degrees are summarized in Figure 3, and the respective Raman spectral data is found in Figures S5 and S6, Supporting Information. It can be
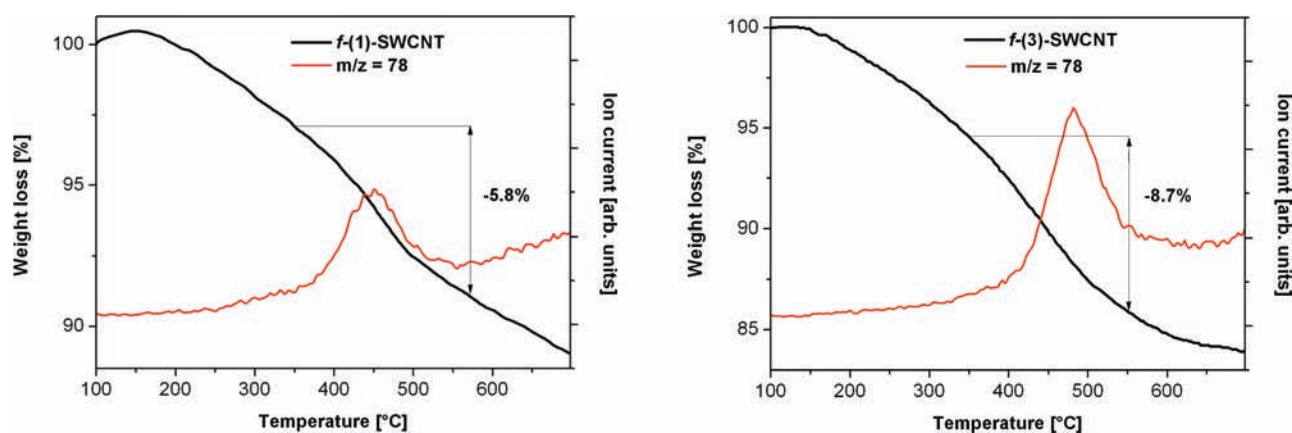
Figure 4. Thermogravimetric profile (weight loss) of *f*-(**1**)-SWCNT (left) and *f*-(**3**)-SWCNT (right); heating rate: 10 K/min. Vertical arrows correspond to the weight loss recorded within the temperature region of phenyl fragment detection (350−570 °C) not corrected by the mass loss of the staring HiPco material. The ion current for $m/z = 78$ ($C_6H_6^+$) is given in arbitrary units.

summarized that the SWCNT sample quality has a significant influence on the reductive functionalization under modified Birch conditions. Nevertheless, commercially available carbon nanotube materials can be used for fast screening studies without the need for time-consuming and tedious SWCNT purification steps.

To further substantiate the Raman-based conclusions on a covalent attachment of the carbonyl-based electrophiles onto the SWCNT scaffold, photoelectron spectroscopic (XPS) investigations of the 1,1,1-trifluoroacetone addition adduct (*f*-(**2**)-SWCNT) and the acylated SWCNT derivative *f*-(**5**)-SWCNT have been carried out. The F 1s core level spectrum of *f*-(**2**)-SWCNT (Figure S7, Supporting Information) exhibits a fluorine content of 0.9% (corrsponding[45] to degree of functionalization of 0.4%), and from the Cl 2p core level spectrum of *f*-(**5**)-SWCNT (Figure S8, Supporting Information) a chlorine content of 1.1% can be derived (corresponding[45] to a degree of functionalization of 0.3%). The emission feature of fluorine is completely absent in the pristine HiPco starting material, whereas a chlorine content of 0.2% was detected. The covalent functional group attachment is further corroborated by the fact that both SWCNT derivatives display a splitting of the O 1s core level accompanied by a substantial increase in the oxygen content in relation to the pristine SWCNT material (Figure S9, Supporting Information). This O 1s core level splitting is a clear indication that the present oxygen functionalities in the HiPco starting material differ in their chemical nature from the oxygen-containing carbonyl functionalities introduced by the addition of the carbonyl-based electrophiles under modified Birch conditions. For a detailed characterization of the respective C 1s core level spectra, a Voigt based fit routine was applied. Herein, for the area of the fitted C−O peak (286.5 eV) in the as received HiPco starting material, a value of 0.04 can be determined, whereas for the area of fitted C=O band (288.2 eV), a value of 0.06 is obtained (Figure S10, Supporting Information). The C 1s fits for *f*-(**5**)-SWCNT yield a C−O peak area of 0.06 and a C=O peak area of 0.1, indicating an increase of C=O species in the sample due to the addition of 3,4-dichlorobezoyl chloride (**5**) (Figure S11, Supporting Information). The C 1s fits for *f*-(**2**)-SWCNT in contrast exhibit a C−O peak area of 0.14 and a C=O peak area of 0.06 indicative of an increase of C−O species due to the transformation of the carbonyl functionality of 1,1,1-trifluoroacetone (**2**) into an alcohol (Figure S12, Supporting Information).

In the case of *f*-(**1**)-SWCNT (Figure 4, left) and *f*-(**3**)-SWCNT (Figure 4, right) sample characterization has also been carried out by means of TGA in combination with the online monitoring of the volatile products by MS.

Herein, the cationic phenyl fragment $C_6H_6^+$ ($m/z = 78$), originating from covalently attached acetophenone and methyl benzoate moieties, can easily be detected in the temperature range between 350 and 570 °C with a pronounced maximum at about 450 °C (see Figure 4). Over the whole heating range (100−700 °C) both samples present a total mass loss of 2.5% and 7.6% (corrected values), respectively. Furthermore, in the temperature range between 350 and 570 °C, attributed to the detachment of the covalently bound addends, *f*-(**1**)-SWCNT and *f*-(**3**)-SWCNT exhibit a mass loss of 5.8% and 8.7%, [2.8% and 6.0% corrected by the mass loss of the unfunctionalized pristine SWCNT starting material, measured as reference (Figure S13, Supporting Information)]. Assuming that the difference in weight between the functionalized derivatives *f*-(**1**)-SWCNT and *f*-(**3**)-SWCNT and the pristine starting material can be correlated with the weight of the detached functional entities and that the residual weight can be attributed to the defunctionalized SWCNTs, a degree of functionalization on the order of 0.3% and 0.8% can be calculated,[26] respectively.

In conclusion, all characterization techniques substantiate the fact that the reaction of ketones and carboxylic acid derivatives with intermediately charged SWCNT anions conducted under the modified Birch conditions yields the corresponding sidewall addition derivatives. The resulting functionalized SWCNT species can directly be used as precursors for the generation of functional SWCNT architectures, as the presented reaction sequence is directly accompanied by an introduction of hydroxyl and keto functionalities, respectively.

Encouraged by these findings we tried to transpose this reaction of negatively charged SWCNT intermediates with carbonyl-based electrophiles to systems where the anionic SWCNT species have been generated by a nucleophilic addition of organolithium compounds, as outlined in Scheme 1a. Therefore, SWCNTs have been dispersed in anhydrous THF by ultrasonic agitation, and the subsequent addition of an excess of *n*-butyl lithium (5 equiv related to mole carbon) yielded the corresponding soluble $(^nBu)_n$-SWCNT^{n-} intermediates. Afterward, the carbonyl-based electrophiles (**1**−**5**) (2 equiv referred
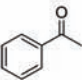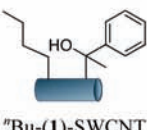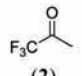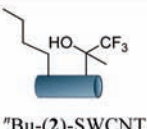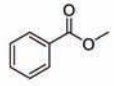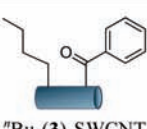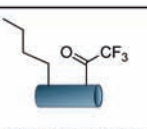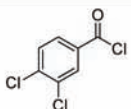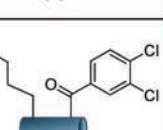
Electrophile (E)	Reductive Functionalization under modified Birch conditions	
(1)	^{n}Bu-(**1**)-SWCNT	A_D/A_G[a]: **1.54** c(NMP): **30 mg/L (30 %)** mass loss (coval.)[b]: **5.6%** mass loss (compl.)[c]: **9.3%** func.degr.: **0.9%**
(2)	^{n}Bu-(**2**)-SWCNT	A_D/A_G[a]: **2.86** c(NMP): **51 mg/L (51 %)**
(3)	^{n}Bu-(**3**)-SWCNT	A_D/A_G[a]: **2.00** c(NMP): **25 mg/L (25 %)** mass loss (coval.)[b]: **1.4%** mass loss (compl.)[c]: **5.1%** func.degr.: **0.2%**
(4)	^{n}Bu-(**4**)-SWCNT	A_D/A_G[a]: **1.80** c(NMP): **66 mg/L (66 %)**
(5)	^{n}Bu-(**5**)-SWCNT	A_D/A_G[a]: **2.08** c(NMP): **31 mg/L (31 %)**

Figure 5. Tabular representation of the different electrophiles, the corresponding SWCNT derivatives after secondary functionalization, the Ram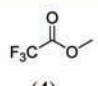an determined A_D/A_G values, the concentration of SWCNTs in the supernatant after mild centrifugation with an initial concentration of 0.1 g/L, and the corresponding dispersion efficiency as well as the TGA-based mass loss together with the corresponding functionalization degree. (a) Values are the ratios $A_{D(sample)}/A_{G(sample)}$ related to A_{D0}/A_{G0} of the pristine HiPco SWCNTs. (b) Mass loss detected by TGA in the temperature range between 350 and 570 °C (covalent detachment of substituents); corrected by the mass loss of the pristine HiPco material. (c) Mass loss over the complete temperature range: 100−700 °C; corrected by the mass loss of the pristine HiPco material.

to the amount of *n*-butyl lithium) were added to the reaction mixture, and the subsequent aqueous workup yielded actually the corresponding mixed functionalized SWCNT derivatives ^{n}Bu-(**1**−**5**)-SWCNT as outlined in Figure 5.

The D-band region (excitation wavelength: 633 nm) of the differently functionalized SWCNT derivatives ^{n}Bu-(**1**−**5**)-SWCNT

is depicted in Figure 5 (the corresponding RBM region and the spectra for 532 and 785 nm excitations are presented in Figures S14−S16, Supporting Information, respectively). Again, the structural alteration of the sp^2 carbon network of the SWCNTs by the covalent attachment of organic moieties can be deduced from the distinct increase of the D-band intensity, detected for all derivatized species, in relation to the pristine starting material.

However, the respective A_D/A_G values are in the same region or slightly higher in comparison to the values calculated for the reductive functionalization under modified Birch conditions (see Figure 1). Therefore, the question arises if the increase in D-band intensity can be attributed to the generation of a double functionalized derivative, with *n*-butyl groups attached alongside with the respective carbonyl-based electrophile, or if just the addition of the nucleophilic butyl group, followed by a reoxidation of the charged (^{n}Bu)$_n$-SWCNT^{n-} species took place.

First evidence for a successful trapping of the anionic (^{n}Bu)$_n$-SWCNT^{n-} intermediates by carbonyl-based electrophiles can be derived from XPS investigations of the fluorine and chlorine containing SWCNT adducts ^{n}Bu-(**2**)-SWCNT (Figure S17, Supporting Information) and ^{n}Bu-(**5**)-SWCNT (Figure S18, Supporting Information). Herein, a fluorine content of 0.6% and a chlorine content of 0.4% could be detected, respectively, indicative for a secondary functionalization by the addition of ketyl radicals generated by an electron-transfer reaction from the primarily established (^{n}Bu)$_n$-SWCNT^{n-} species.

This is unambiguously substantiated by the TGA/MS-based analysis of the mixed functionalized SWCNT derivatives ^{n}Bu-(**1**)-SWCNT (depicted in Figure 6, right) and ^{n}Bu-(**3**)-SWCNT (Figure S19, Supporting Information). In both derivatives the presence of phenyl fragments $C_6H_6^+$ ($m/z = 78$) can be detected in the temperature range between 350 and 570 °C, concomitant with the registration of the mass trace of butyl cations $C_4H_9^+$ ($m/z = 57$). In addition, the mass loss values (5.6%, ^{n}Bu-(**1**)-SWCNT and 1.4%, ^{n}Bu-(**3**)-SWCNT) are in a comparable range as the mass losses detected for the corresponding derivatives *f*-(**1**)-SWCNT and *f*-(**3**)-SWCNT derived under modified Birch conditions.

As already outlined within this manuscript, the degree of functionalization under modified Birch conditions (scheme 1a) is dependent on the eletrophilicity of the addend species. This is in marked contrast to the subsequent nucleophilic attack of the ^{n}Bu anion and the trapping of the negative charges on the SWCNT scaffold with the respective electrophiles in a SET mechanism (scheme 1b), where a different trend is observed. This is traced back to the complex nature of the double functionalization sequence—nucleophilic addition with subsequent electrophilic functionalization—which is in addition accompanied by a convolution of an intermediately established equilibrium, previously investigate by our group.[26] As outlined in Figure 7, a dominant contribution from this underlying equilibrium (**I**, **II**) can be expected on the subsequent attack of the carbonyl-based electrophiles (**E**).

In a side reaction, the excess of the added electrophilic carbonyl compounds (**E**) (2 equiv referred to the amount of *n*-butyl lithium) will react with free *n*-butyl lithium, present in the SWCNT/nucleophile equilibrium (**I**, **II**), yielding the corresponding addition product *n*-butyl-*E* (**III**). This leads to a decrease of the concentration of *n*-butyl anions in the solution, which is directly coupled to a shift of the equilibrium toward alkylated (^{n}Bu)$_{n-x}$SWCNT$^{(n-x)-}$ species with lower degrees of functionalization (**IV**), in terms of the primary *n*-butyl addend.
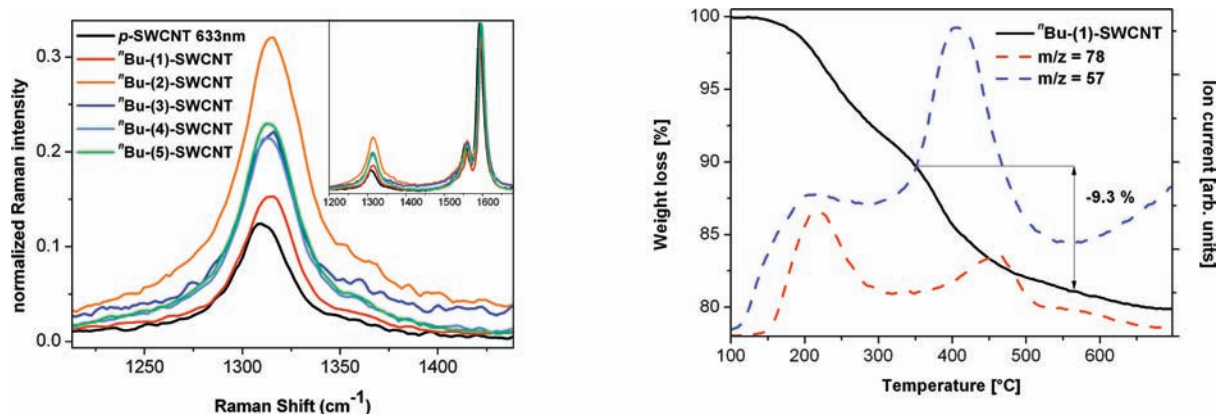
Figure 6. (Left): Raman spectra (633 nm excitation) of pristine SWCNTs (black trace) and functionalized SWCNT derivatives ^{n}Bu-(**1**−**5**)-SWCNT (color coded) after secondary electrophilic functionalization of intermediately generated (^{n}Bu)$_n$-SWCNT^{n-} species. (Right): Thermogravimetric profile (weight loss) of ^{n}Bu-(**1**)-SWCNT; heating rate: 10 K/min. Vertical arrows correspond to the weight loss recorded within the temperature region of phenyl and n-butyl fragment detection (350−550 °C); not corrected by the mass loss of the staring HiPco material. The ion current for $m/z = 78$ ($C_6H_6{}^+$) and $m/z = 57$ ($C_4H_9{}^+$) is given in arbitrary units.

This functional group detachment also decreases the charge concentration on the anionic SWCNT intermediates and therefore reduces the inherent driving force for the final SET reactions from the carbon nanotubes to the carbonyl-based electrophiles, yielding the corresponding addition product (**V**). Furthermore, this equilibrium reaction will be favored for stronger electrophilic interception reagents. Nevertheless, the reaction kinetics between n-butyl lithium and the various carbonyl species (ketones, esters, and carboxylic acid chlorides) differs in wide ranges and is directly related to the equilibrium position (**III**, **IV**) of the intermediately generated (^{n}Bu)$_n$SWCNT^{n-} species. Therefore, a direct comparison of the functionalization degrees reached by the modified Birch reaction (mono adduct generation) and obtained by the double functionalization sequence is not possible.

Nevertheless, both derivatization sequences yield materials with a pronounced solubility in organic solvents, like NMP. This enabled us to investigate the influence of the covalent SWCNT sidewall functionalization onto the excitonic transition features of carbon nanotubes. It has been outlined by Tour et al. that the structural modification of the sp^2 π-system associated with the covalent attachment of substituents leads to an almost complete loss of the UV−vis/nIR excitonic transitions being related to the van Hove singularities in the density of states of SWCNTs.[54,55] Therefore, the absence of these transitions has widely been taken as a criterion for covalent sidewall functionalization. However, it has also been reported that mild functionalization does not induce a complete depletion of these characteristic transitions.[18,19,21,23,25,32,38,43,56,57] This is in total agreement with our observations. The corresponding absorption spectra of f-(**1**−**5**)-SWCNTs, normalized to 930 nm, are depicted in Figure 8a (for ^{n}Bu-(**1**−**5**)-SWCNTs see Figure S20, Supporting Information). The characteristic excitonic transitions are clearly discernible throughout all SWCNT derivatives, spanning a A_D/A_G ratio range from 1.13 (f-(**1**)-SWCNT) to 2.36 (f-(**4**)-SWCNT). Therefore, the functionalization degree threshold for a complete loss of the van Hove-based excitonic transition has to be located above this value. Interestingly, we also observed a blue shift of the excitonic transitions in comparison to the HiPco starting material (Figure 8b). We suppose that this is traced back to more efficient debundling in NMP due to the introduction of functional entities on
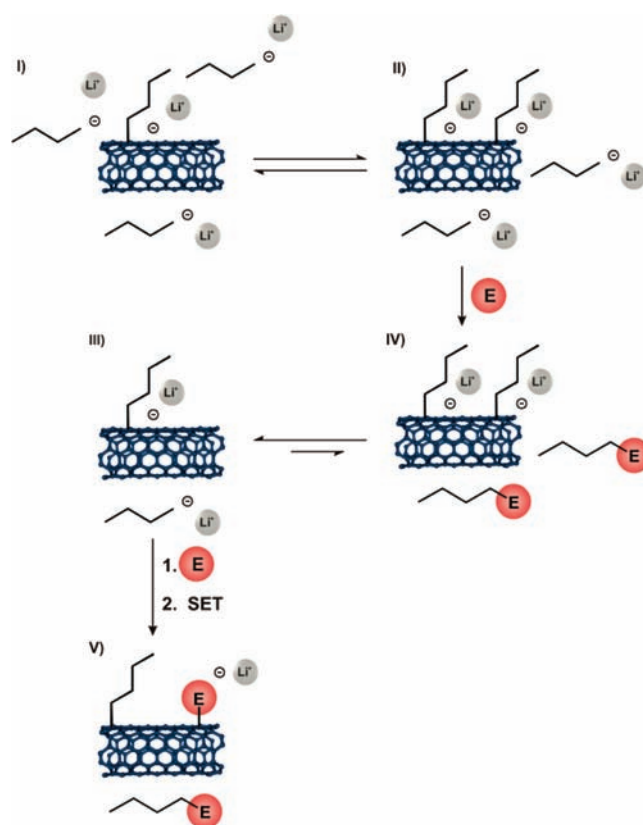
Figure 7. Intermediate (^{n}Bu)$_n$-SWCNT^{n-} defunctionalization by electrophiles, based on the reversibility of the initial nucleophilic addition reaction on SWCNTs.

the nanotube sidewall,[58,59] as the extent of the observed blue shift, ranging from 46−200 cm^{-1}, roughly correlates with the degree of functionalization, determined by the Raman A_D/A_G ratios.

Encouraged by the absorption spectroscopic investigation, we have also subjected the samples to emission spectroscopy after diluting the dispersions to the same SWCNT concentration (0.01 g/L), even though covalent functionalization induces a loss of the SWCNT nIR-fluorescence features.[60−62]

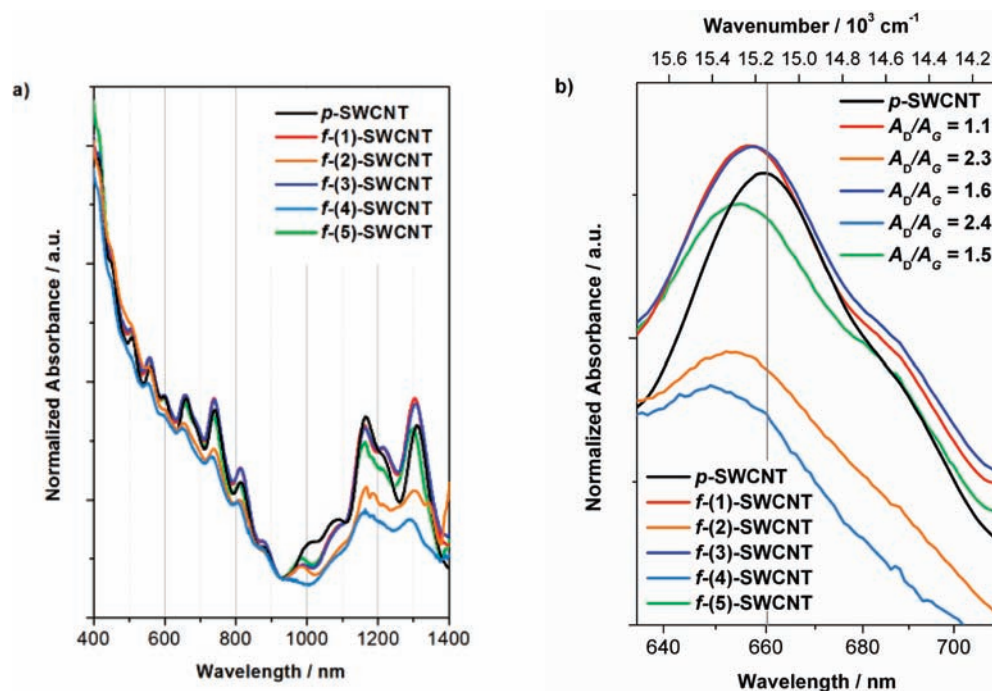**Figure 8.** (a) UV–vis/nIR absorption spectra of the supernatant after centrifugation of SWCNT derivatives *f*-(**1**–**5**)-SWCNT in NMP (initial concentration 0.1 g/L, normalized to 930 nm). (b) Detailed visualization of the absorption peaks centered at 660 nm with the corresponding Raman A_D/A_G values as inset.
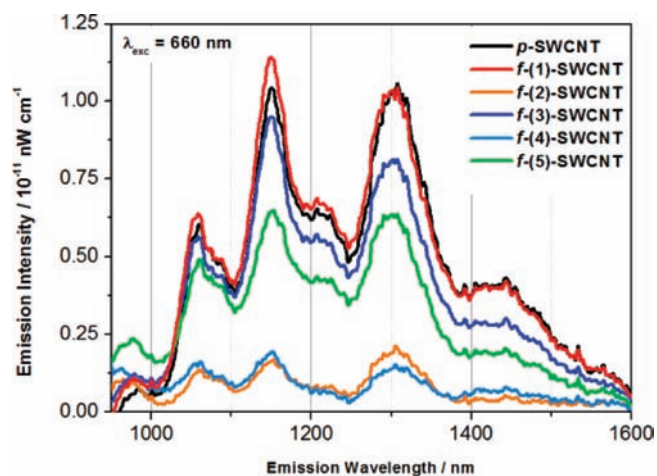

Figure 9. (a) nIR emission spectra of *f*-(**1**-**5**)-SWCNT dispersed in NMP at λ_{ex} = 660 nm (baseline corrected). In all cases, the supernatant after centrifugation was diluted to an optical density of 0.34 cm^{-1} at 660 nm.

As outlined above, our mild functionalization does not completely destroy the optical properties of the SWCNTs, so that residual nIR-emission is detected, as exemplarily depicted for *f*-(**1**–**5**)-SWCNTs in Figure 9a, excitation wavelength of 660 nm (for ^{n}Bu-(**1**–**5**)-SWCNTs see Figure S21, Supporting Information).

The emission intensity at 1150 nm of the functionalized material relative to the emission intensity of the starting material $(I_{\mathrm{Em}}(f\text{-}(\mathbf{1}\text{–}\mathbf{5})\text{-SWCNT})/I_{\mathrm{Em}}(p\text{-SWCNT}))$, processed under equal experimental conditions, can be taken as a measure for the functionalization induced loss of the SWCNT fluorescence. As outlined in Figure S22a, Supporting Information, the Raman

A_D/A_G ratio is in good agreement with the decrease in SWCNT fluorescence upon the attachment of covalently bound addends, e.g., the emission intensity decreases approximately linearly with an increasing A_D/A_G ratio. However, as only individualized semiconducting SWCNTs exhibit nIR fluorescence, the changes in nanotube emission intensities could also be traced back to varying degrees of nanotube exfoliation.

In order to address the issue of nanotube aggregation, the samples *f*-(**2**)-SWCNT and ^{n}Bu-(**2**)-SWCNTs were subjected to microscopic characterization (for detailed information see Supporting Information). The atomic force microscopic height analysis (Figures S23–S25, Supporting Information) of the SWCNT samples reveals that the functionalized nanotubes dispersed in NMP are characterized by a significantly higher degree of individualization and smaller aggregates on average, especially in the case of *f*-(**2**)-SWCNT compared to the pristine SWCNTs. Additionally no shortening of the functionalized nanotubes due to the ultrasonic agitation can be detected.

Even though the differences in the population of the exfoliated nanotubes also affect the emission intensity ratio (Figure S22a, Supporting Information), resulting in a deviation from the linear progression, the decrease in nIR emission with respect to the pristine material can be attributed to the covalent functionalization, as nanotube individualization is more pronounced.

Interestingly, the nanotube dispersibility in NMP also decreases approximately linearly with increasing degrees of functionalization in the sample *f*-(**1**–**5**)-SWCNT (see Figure S22b, Supporting Information). As already outlined by Coleman and co-workers,[43,63] covalent functionalization may lead to a decreased dispersibility in this solvent, as the solubility properties of the sidewall derivatized material are dominated by the nature of the functional entity and no longer by the nanotube scaffold. This explanation is totally consistent with the behavior of our sidewall

functionalized material. Roughly, a similar trend is observed for ^nBu-$(\mathbf{1}-\mathbf{5})$-SWCNT. For this system, a direct correlation between the functionalization degree of the system, the ratio of the different addends, and the related optical properties is highly challenging, so that an in depth investigation deserves further attention. An extended study related to that subject in combination with the investigation of the individualization degrees is currently underway in our laboratory.

CONCLUSION

In the present work, we have shown that a broad variety of carbonyl-based electrophiles—ketones, esters, carboxylic acid chlorides—can be used for the covalent SWCNT sidewall functionalization under modified Birch conditions. The degree of functionalization accessible by this reaction sequence directly correlates with the stability/reactivity of the intermediately generated ketyl radical species. Furthermore, carbonyl compounds can also be used for the electrophilic trapping of negatively charged intermediates obtained by the nucleophilic attack of organolithium species. This directly leads to the formation of mixed functional SWCNT derivatives. Functionalization degrees of this organometallic reduction approach are lower compared to the respective monofunctionalization under modified Birch conditions and can be explained by an equilibrium based, partial defunctionalization of the alkylated anionic SWCNT intermediates. This directly leads to a decrease of the charge concentration on the SWCNT scaffold and reduces the inherent driving force for the ketyl radical formation by a single electron-transfer reaction with reduced SWCNT species as donor components. In spite of the alteration of the sp^2 carbon network by the covalent attachment of the respective ketyl radicals, all derivatives still exhibit pronounced optical transitions. Based on a detailed investigation of the absorption and the emission features, a direct correlation between the functionalization degree and the UV−vis/nIR absorption and nIR fluorescence intensity becomes evident. The expansion of sidewall functionalization reagents toward carbonyl compounds can be seen as a substantial step forward for the development of nanotube-based materials, as the introduced hydroxyl and carbonyl groups may conveniently be used as coupling units for the connection of functional entities.

ASSOCIATED CONTENT

S **Supporting Information.** EPR blind test investigations, Raman spectra of f-$(\mathbf{1}-\mathbf{5})$-SWCNT (532 nm, 785 nm excitation), Raman spectra of microwave purified pf-$(\mathbf{1},\mathbf{3})$-SWCNT thermal purified pf-$(\mathbf{1},\mathbf{3})$-SWCNT, Raman spectra of ^nBu-$(\mathbf{1}-\mathbf{5})$-SWCNT (RBM 633 nm, 532 nm, 785 nm excitation), XPS spectra and C 1s fits of p-(SWCNT) and f-$(\mathbf{2},\mathbf{5})$-SWCNT, TGA characterization of the starting material, TH-SWCNT and MW-SWCNT, TGA/MS profiles of ^nBu-$(\mathbf{3})$-SWCNT, UV−vis/nIR absorption spectra of ^nBu-$(\mathbf{1}-\mathbf{5})$-SWCNT and, nIR emission spectra of ^nBu-$(\mathbf{1}-\mathbf{5})$-SWCNT. This material is available free of charge via the Internet at http://pubs.acs.org.

AUTHOR INFORMATION

Corresponding Author

*andreas.hirsch@chemie.uni-erlangen.de.

REFERENCES

(1) Kroto, H. W.; Heath, J. R.; O'Brien, S. C.; Curl, R. F.; Smalley, R. E. *Nature* **1985**, *318*, 162.

(2) Iijima, S. *Nature* **1991**, *354*, 56.

(3) Bethune, D. S.; Kiang, C. H.; de Vries, M. S.; Gorman, G.; Savoy, R.; Vazquez, J.; Beyers, R. *Nature* **1993**, *363*, 605.

(4) Iijima, S.; Ichihashi, T. *Nature* **1993**, *363*, 603.

(5) Novoselov, K. S.; Geim, A. K.; Morozov, S. V.; Jiang, D.; Zhang, Y.; Dubonos, S. V.; Grigorieva, I. V.; Firsov, A. A. *Science* **2004**, *306*, 666.

(6) Dresselhaus, M. S.; Dresselhaus, G.; Avouris, P. *Carbon Nanotubes: Synthesis, Structure, Properties, and Applications*; Springer: Berlin, Germany, 2001.

(7) Jorio, A.; Dresselhaus, G.; Dresselhaus, M. S. *Top. Appl. Phys.* **2008**, *111*.

(8) Baughman, R. H.; Zakhidov, A. A.; de Heer, W. A. *Science* **2002**, *297*, 787.

(9) Ausman, K. D.; Piner, R.; Lourie, O.; Ruoff, R. S.; Korobov, M. *J. Phys. Chem. B* **2000**, *104*, 8911.

(10) Bahr, J. L.; Mickelson, E. T.; Bronikowski, M. J.; Smalley, R. E.; Tour, J. M. *Chem. Commun.* **2001**, 193.

(11) Tasis, D.; Tagmatarchis, N.; Bianco, A.; Prato, M. *Chem. Rev.* **2006**, *106*, 1105.

(12) Hirsch, A.; Vostrowsky, O. *Functionalization of carbon nanotubes*; Wiley-VCH Verlag: Weinheim, Germany, 2007.

(13) Peng, X.; Wong, S. S. *Adv. Mater.* **2009**, *21*, 625.

(14) Singh, P.; Campidelli, S.; Giordani, S.; Bonifazi, D.; Bianco, A.; Prato, M. *Chem. Soc. Rev.* **2009**, *38*, 2214.

(15) Hauke, F.; Hirsch, A. In *Carbon Nanotubes and Related Structures*; Guldi, D. M., Martin, N., Eds.; Wiley-VCH: Weinheim, Germany, 2010, p 135.

(16) Graupner, R.; Hauke, F. In *The Oxford Handbook of Nanoscience and Technology*; Narlikar, A. V., Fu, Y. Y., Eds.; Oxford University Press: New York, 2010, p 508.

(17) Graupner, R.; Abraham, J.; Wunderlich, D.; Vencelova, A.; Lauffer, P.; Roehrl, J.; Hundhausen, M.; Ley, L.; Hirsch, A. *J. Am. Chem. Soc.* **2006**, *128*, 6683.

(18) Syrgiannis, Z.; Hauke, F.; Röhrl, J.; Hundhausen, M.; Graupner, R.; Elemes, Y.; Hirsch, A. *Eur. J. Org. Chem.* **2008**, 2544.

(19) Gebhardt, B.; Graupner, R.; Hauke, F.; Hirsch, A. *Eur. J. Org. Chem.* **2010**, 1494.

(20) Wunderlich, D.; Hauke, F.; Hirsch, A. *Chem.—Eur. J.* **2008**, *14*, 1607.

(21) Viswanathan, G.; Chakrapani, N.; Yang, H.; Wei, B.; Chung, H.; Cho, K.; Ryu Chang, Y.; Ajayan Pulickel, M. *J. Am. Chem. Soc.* **2003**, *125*, 9258.

(22) Blake, R.; Gun'ko, Y. K.; Coleman, J.; Cadek, M.; Fonseca, A.; Nagy, J. B.; Blau, W. J. *J. Am. Chem. Soc.* **2004**, *126*, 10226.

(23) Bayazit, M. K.; Suri, A.; Coleman, K. S. *Carbon* **2010**, *48*, 3412.

(24) Roubeau, O.; Lucas, A.; Penicaud, A.; Derre, A. *J. Nanosci. Nanotechnol.* **2007**, *7*, 3509.

(25) Maeda, Y.; Kato, T.; Hasegawa, T.; Kako, M.; Akasaka, T.; Lu, J.; Nagase, S. *Org. Lett.* **2010**, *12*, 996.

(26) Syrgiannis, Z.; Gebhardt, B.; Dotzer, C.; Hauke, F.; Graupner, R.; Hirsch, A. *Angew. Chem., Int. Ed.* **2010**, *49*, 3322.

(27) Liang, F.; Sadana, A. K.; Peera, A.; Chattopadhyay, J.; Gu, Z.; Hauge, R. H.; Billups, W. E. *Nano Lett.* **2004**, *4*, 1257.

(28) Liang, F.; Alemany, L. B.; Beach, J. M.; Billups, W. E. *J. Am. Chem. Soc.* **2005**, *127*, 13941.

(29) Chattopadhyay, J.; Sadana, A. K.; Liang, F.; Beach, J. M.; Xiao, Y.; Hauge, R. H.; Billups, W. E. *Org. Lett.* **2005**, *7*, 4067.

(30) Stephenson, J. J.; Sadana, A. K.; Higginbotham, A. L.; Tour, J. M. *Chem. Mater.* **2006**, *18*, 4658.

(31) Billups, W. E.; Liang, F.; Chattopadhyay, J.; Beach, J. M. *ECS Transactions* **2007**, *2*, 65.

(32) Wunderlich, D.; Hauke, F.; Hirsch, A. *J. Mater. Chem.* **2008**, *18*, 1493.

(33) Mukherjee, A.; Combs, R.; Chattopadhyay, J.; Abmayr, D. W.; Engel, P. S.; Billups, W. E. *Chem. Mater.* **2008**, *20*, 7339.

(34) Chattopadhyay, J.; Chakraborty, S.; Mukherjee, A.; Wang, R.; Engel, P. S.; Billups, W. E. *J. Phys. Chem. C* **2007**, *111*, 17928.

(35) Borondics, F.; Bokor, M.; Matus, P.; Tompa, K.; Pekker, S.; Jakab, E. *Fullerenes, Nanotubes, Carbon Nanostruct.* **2005**, *13*, 375.

(36) Borondics, F.; Jakab, E.; Pekker, S. *J. Nanosci. Nanotechnol.* **2007**, *7*, 1551.

(37) Martinez-Rubi, Y.; Guan, J.; Lin, S.; Scriver, C.; Sturgeon, R. E.; Simard, B. *Chem. Commun.* **2007**, 5146.

(38) Voiry, D.; Roubeau, O.; Penicaud, A. *J. Mater. Chem.* **2010**, *20*, 4385.

(39) Guan, J.; Martinez-Rubi, Y.; Denommee, S.; Ruth, D.; Kingston, C. T.; Daroszewska, M.; Barnes, M.; Simard, B. *Nanotechnology* **2009**, *20*, 245701/1.

(40) Garcia-Gallastegui, A.; Obieta, I.; Bustero, I.; Imbuluzqueta, G.; Arbiol, J.; Miranda, J. I.; Aizpurua, J. M. *Chem. Mater.* **2008**, *20*, 4433.

(41) Chajara, K.; Andersson, C.-H.; Lu, J.; Widenkvist, E.; Grennberg, H. *New J. Chem.* **2010**, *34*, 2275.

(42) Chiang, I. W.; Brinson, B. E.; Huang, A. Y.; Willis, P. A.; Bronikowski, M. J.; Margrave, J. L.; Smalley, R. E.; Hauge, R. H. *J. Phys. Chem. B* **2001**, *105*, 8297.

(43) Amiran, J.; Nicolosi, V.; Bergin, S. D.; Khan, U.; Lyons, P. E.; Coleman, J. N. *J. Phys. Chem. C* **2008**, *112*, 3519.

(44) Backes, C.; Englert, J.; Bernhard, N.; Hauke, F.; Hirsch, A. *Small* **2010**, *6*, 1968.

(45) Abraham, J. University of Erlangen-Nürnberg, 2005.

(46) Wei, L.; Zhang, Y. *Chem. Phys. Lett.* **2007**, *446*, 142.

(47) Dresselhaus, M. S.; Dresselhaus, G.; Jorio, A.; Souza Filho, A. G.; Pimenta, M. A.; Saito, R. *Acc. Chem. Res.* **2002**, *35*, 1070.

(48) Dresselhaus, M. S.; Dresselhaus, G.; Saito, R.; Jorio, A. *Phys. Rep.* **2005**, *409*, 47.

(49) Graupner, R. *J. Raman Spectrosc.* **2007**, *38*, 673.

(50) Mueller, M.; Maultzsch, J.; Wunderlich, D.; Hirsch, A.; Thomsen, C. *Phys. Status Solidi B* **2007**, *244*, 4056.

(51) Mueller, M.; Maultzsch, J.; Wunderlich, D.; Hirsch, A.; Thomsen, C. *Phys. Status Solidi RRL* **2007**, *1*, 144.

(52) Xu, Y.-Q.; Peng, H.; Hauge, R. H.; Smalley, R. E. *Nano Lett.* **2005**, *5*, 163.

(53) Wang, Y.; Shan, H.; Hauge, R. H.; Pasquali, M.; Smalley, R. E. *J. Phys. Chem. B* **2007**, *111*, 1249.

(54) Bahr, J. L.; Tour, J. M. *Chem. Mater.* **2001**, *13*, 3823.

(55) Bahr, J. L.; Yang, J.; Kosynkin, D. V.; Bronikowski, M. J.; Smalley, R. E.; Tour, J. M. *J. Am. Chem. Soc.* **2001**, *123*, 6536.

(56) Guldi, D. M.; Rahman, G. M. A.; Qin, S.; Tchoul, M.; Ford, W. T.; Marcaccio, M.; Paolucci, D.; Paolucci, F.; Campidelli, S.; Prato, M. *Chem.—Eur. J.* **2006**, *12*, 2152.

(57) Georgakilas, V.; Bourlinos, A.; Gournis, D.; Tsoufis, T.; Trapalis, C.; Mateo-Alonso, A.; Prato, M. *J. Am. Chem. Soc.* **2008**, *130*, 8733.

(58) Cathcart, H.; Quinn, S.; Nicolosi, V.; Kelly, J. M.; Blau, W. J.; Coleman, J. N. *J. Phys. Chem. C* **2007**, *111*, 66.

(59) Arnold, M. S.; Guler, M. O.; Hersam, M. C.; Stupp, S. I. *Langmuir* **2005**, *21*, 4705.

(60) Cognet, L.; Tsyboulski, D. A.; Rocha, J.-D. R.; Doyle, C. D.; Tour, J. M.; Weisman, R. B. *Science* **2007**, *316*, 1465.

(61) Strano, M. S.; Huffman, C. B.; Moore, V. C.; O'Connell, M. J.; Haroz, E. H.; Hubbard, J.; Miller, M.; Rialon, K.; Kittrell, C.; Ramesh, S.; Hauge, R. H.; Smalley, R. E. *J. Phys. Chem. B* **2003**, *107*, 6979.

(62) Siitonen Anni, J.; Tsyboulski Dmitri, A.; Bachilo Sergei, M.; Weisman, R. B. *Nano Lett.* **2010**, *10*, 1595.

(63) Coleman, J. N. *Adv. Funct. Mater.* **2009**, *19*, 3680.